Distribution and size fractionation of nickel and cobalt species along the Amazon estuary and mixing plume

Leandro M. de Carvalho[1]*, Adrienne Patricia Hollister[2], Cristina Trindade[1], Martha Gledhill[3] and Andrea Koschinsky[2]

[1] *Department of Chemistry, Federal University of Santa Maria (UFSM), Santa Maria-RS, Brazil.*

[2] *Department of Physics and Earth Science, Jacobs University Bremen, Campus Ring, 28759 Bremen, Germany.*

[3] *GEOMAR - Helmholtz Centre for Ocean Research Kiel, 24148 Kiel, Germany.*

* Corresponding author. E-mail: lemacarvalho@gmail.com

Department of Chemistry, Federal University of Santa Maria (UFSM), Santa Maria-RS, Brazil, PO Box 5051, Zip Code 97105-970, Santa Maria-RS, Brazil

ABSTRACT

The Amazon River has the largest drainage basin in the world, making it a major source of trace elements and dissolved organic matter (DOM) to the Atlantic Ocean. However, despite the increasing anthropogenic impacts to the Amazon basin, few recent studies exist quantifying trace element data in this region. The aim of the study was to analyze the input and removal processes that influence the transport of Ni and Co species in the Amazon and Pará River estuaries and mixing zone. Toward this goal, this work provides a comprehensive mixing and speciation study for the trace elements Ni and Co. Samples were collected during a period of high river discharge on the RV Meteor cruise M147 (Amazon – GEOTRACES process study GApr11) in the Amazon and Pará River outflow regions, as well as the aging mixing plume to the north, a mangrove belt to the southeast and the North Brazil Current (NBC) seawater endmember. Here we present the results for labile particulate (>0.2 μm), labile and total dissolved (<0.2 μm), large colloidal (0.015-0.2 μm), soluble (<0.015 μm) and ultrafiltered (<1 and <10 kDa) fractions of Ni and Co in surface waters (towed-fish) and along the water column at different depths (CTD) samples using comparative approaches by adsorptive cathodic stripping voltammetry (AdCSV) and inductively coupled plasma-mass spectrometry (ICP-MS). We observed good agreement between AdCSV and ICP-MS measurements for Ni, and to a lesser extent Co. In general, dissolved and soluble Ni and Co decreased with increasing salinity, however additional non-conservative removal was also observed and attributed to possible biological uptake and colloidal flocculation. Shipboard AdCSV measurements showed that dissolved Ni was present mostly in the "reactive" form as weak complexes, suggesting high bioavailability, while reactive dissolved Co was absent, indicating the presence of strong organic Co complexes. In both Ni and Co, an elevated colloidal fraction was observed at low salinity, suggesting removal of dissolved Ni and Co via colloidal flocculation upon seawater mixing, while the soluble species were transported to the Atlantic Ocean. At depth, the soluble phase dominated, and we observed concentration maxima at 500-1000 m, indicating the presence of Antarctic Intermediate Water (AIW) and possible biological regeneration. We also observed unique source signatures in dissolved and labile particulate Ni and Co species from the Amazon and Pará River outflow regions, in addition to a contribution from mangrove belt-associated groundwater.

1. Introduction

The transport of elements from rivers to the ocean in estuarine mixing zones is governed by a variety of different physicochemical and biological processes. In general, only a fraction of the total content of trace elements reaches the ocean due to the aggregation and flocculation processes that trap metals in estuarine sediments during estuarine mixing (Boyle et al., 1977; Sholkovitz, 1978; Hunter, 1983; Mosley and Liss, 2020). The formation of stable organic complexes with dissolved organic matter (DOM) can increase trace element solubility and riverine metal flux into the ocean (Dittmar et al., 2006), and as most tropical rivers such as the Amazon River are very rich in DOM, organic complexation plays a prominent role in these systems. Moreover, the removal of trace elements in mixing zones is strongly linked to distribution among different colloidal structures and smaller size fractions (<0.015 μm, <10 kDa and <1 kDa). Trace elements associated with organic and inorganic colloids are strongly affected by coagulation and physical removal, while smaller structures (<0.015 μm) and truly dissolved metals (<10 kDa) normally pass through the estuarine mixing zone and reach the open ocean without removal (Stolpe and Hassellöv, 2007; Pokrovsky et al., 2014).

Studies to understand the trace element transport mechanisms in river-seawater mixing zones have been conducted in tropical estuaries worldwide (Boyle et al., 1982; DeMaster et al., 1991; Seyler and Boaventura, 2003; Fu et al., 2012;), but data from the Amazon River estuary remain sparse (Boyle et. al, 1982; Smoak et al., 2006; Hollister et. al, 2021). The Amazon River has the largest average discharge (150,500 m³ s⁻¹) and drainage basin in the world, accounting for about one fifth of Earth's total river flow into the ocean (Espinoza Villar et al., 2009) and acting as the major source of dissolved trace elements and DOM to the Atlantic Ocean. Additionally, a high load of particulate material is discharged and partially settles in the Amazon estuary (DeMaster et al., 1991; Seyler et al., 2003). The Amazon River basin has been increasingly subject to anthropogenic pressures, including climate change, deforestation, hydroelectric damming and terrestrial mining (Davidson et al., 2012). Some of these changes, including mining and forest fires, are known to alter trace element concentrations in rivers and sediments of the Amazon catchment area (Yamasoe et al., 2000; Lacerda et al., 2004; Cesar et al. 2011; Guimberteau et al. 2017). Furthermore, climate change is projected to alter river discharge, causing both increased droughts and flooding in different areas of the basin (Guimberteau et al., 2013). Given the relevance of the Amazon River and its volume output to the Atlantic, a thorough investigation of the interactions and distribution patterns of trace

elements and DOM in the estuary and freshwater plume is imperative to establish current levels of trace element concentrations to assess future changes.

The transition metals play important roles in ocean biogeochemistry mainly due to their involvement in photosynthetic carbon fixation by marine phytoplankton and metabolic processes (Archer et. al, 2020). Among these metals, nickel (Ni) and cobalt (Co) are well-known essential micronutrients and can even be limiting or colimiting to phytoplankton growth in some ocean regimes (Price and Morel, 1991; Achterberg et al. 1997; Saito and Moffett, 2002; Saito and Geopfert, 2008; Dupont et al., 2010; Browning et al., 2017). Cobalt is extensively complexed by organic ligands (Saito and Moffett 2001, Ellwood and Van den Berg 2001, Bown et al., 2012), accounting for >99% of dissolved Co in some surface waters (Bown et al., 2012). These ligands may enhance Co bioavailability to some phytoplankton (e.g. cyanobacteria) while limiting bioavailability to others (e.g. diatoms) (Saito et al. 2002, Saito et al. 2005). On the other hand, Ni is only ~30-50% organically complexed in seawater (Van den Berg and Nimmo 1987, Nimmo et al. 1989, Boiteau et al. 2016). Thus, understanding Ni and Co biogeochemistry in estuaries and mixing zones requires an understanding of their physicochemical speciation, including lability and size fractionation (e.g. labile particulate, dissolved, colloidal, and truly dissolved fractions) to determine bioavailable metal content.

Methods for quantifying trace elements in seawater and estuaries have primarily centered on trace element preconcentration followed by inductively coupled plasma-mass spectrometry (ICP-MS) (Sohrin et al. 2008, Milne et al., 2010; Pöhle et al., 2015; Rapp et al., 2017). Apart from the well-established use of these spectrometric techniques, different electrochemical approaches have also been used for the quantification of total dissolved concentrations and analysis of trace element speciation in seawater and freshwater (Van den Berg and Nimmo, 1987; Muratt et al., 2015; Cabanesa et al., 2020). For example, cathodic or anodic stripping voltammetry (SV) techniques have demonstrated high sensitivity and selectivity in studies involving the redox and physicochemical speciation of elements at low concentrations (Van den Berg and Nimmo, 1987; Muratt et al., 2015; Cabanesa et al., 2020). In addition, the application of SV is advantageous due to its ability to determine distinct chemical fractions (i.e. electrochemically reactive species). Furthermore, SV analysis can be carried out shipboard, minimizing alterations in the chemical speciation due to long-term sample storage. This is especially relevant for the analyses of estuarine samples which span a wide range of salinities from freshwater to seawater over the mixing gradient. For electrochemical analysis of Ni and Co, dioxime complexes have been exploited in natural water systems over recent years (Van den Berg and Nimmo, 1987; Donat et al., 1994; Saito and Moffett, 2001; Xue et al., 2001).

124 Dimethylglyoxime (DMG) complexes, characterized by the presence of oxime groups, provide

125 enhancement of Ni(II) and Co(II) voltammetric signals relative to the reduction of the free Ni^{2+}

126 and Co^{2+} cations and other electroactive organic ligands. In addition, DMG complexes of Ni(II)

127 and Co(II) in buffered alkaline electrolytes have good stability compared to other complexing

128 media (Muratt et al., 2015).

129   Here we present a comprehensive speciation study of Ni and Co in water samples from

130 the Amazon and Pará River estuaries and surrounding regions of the Northwest Brazilian

131 Continental Shelf. Samples were collected during the RV Meteor cruise M147 (Amazon -

132 GEOTRACES process study GApr11) in April–May 2018 during a period of high river

133 discharge in order to investigate trace element and organic matter behavior in the Amazon and

134 Pará River outflow regions and mixing zones. Speciation analyses of Ni and Co were conducted

135 shipboard using adsorptive cathodic stripping voltammetry (AdCSV). Comparative

136 concentration measurements were then carried out in home laboratories using both AdCSV and

137 ICP-MS with SeaFAST preconcentration. We separated Ni and Co species based on size and

138 chemical lability and we present the results for labile particulate (>0.2 μm), labile and total

139 dissolved (<0.2 μm), large colloidal (0.015-0.2 μm), soluble (<0.015 μm) and ultrafiltered (<1

140 and <10 kDa) fractions. Our size fractions were chosen based on protocols outlined in the

141 GEOTRACES program (Cutter et al., 2017) and whilst they do not map directly onto

142 particulate, colloidal and truly dissolved fractions, we hypothesized that they would

143 nevertheless provide insight into size partitioning of Ni and Co in our study region. We use the

144 obtained distributions of the physical and chemically defined Ni and Co fractions to provide

145 insight into the input and removal processes that influence transport of Ni and Co species along

146 this highly dynamic region.

147

148

2. Materials and Methods

2.1 Apparatus

The voltammetric measurements performed shipboard of the research vessel FS Meteor were carried out using a 746 VA Trace Analyzer in combination with the VA Stand 694 (Metrohm, Herisau, Switzerland). The voltammetric measurements performed in the home laboratory were carried out by using an Autolab potentiostat (PGSTAT302N) in combination with the VA Stand 663 (Metrohm, Herisau, Switzerland). The surface area of the hanging mercury drop electrode (HMDE) was 0.6 mm^2. The working cells consisted of three electrodes: a mercury multimode electrode (MME) with a HMDE as the working electrode, Ag/AgCl (3 mol L^{-1} KCl) as the reference electrode, and a platinum wire as the auxiliary electrode (all from Metrohm). The ICP-MS measurements were performed on a Thermo Element XR ICP-MS (Thermo Fisher Scientific, MA, USA), and preconcentration was performed on an Element Scientific Inc. (ESI) SeaFAST (SeaFAST-Pico^{TM}). Sample digestion by UV irradiation was performed on a homemade digester equipped with a low-pressure mercury lamp prior to SeaFAST preconcentration and ICP-MS analysis (Rapp et al., 2017; Hollister et al., 2021). A homemade UV device equipped with a high-pressure mercury lamp (400W) was used for AdCSV analysis, as described elsewhere (Carvalho et al., 2008).

2.2 Reagents and solutions

All acids and chemicals were of analytical ultra-pure grade. The water used to prepare all solutions was purified through a Milli-Q system (18.2 MΩ cm^{-1}; Millipore, Bedford, MA, USA).

For voltammetric analyses, dimethylglyoxime (DMG) was obtained from Sigma-Aldrich (St. Louis, MO). Concentrated ammonia solution (25%, w/w), nitric acid (HNO$_3$; 65%, w/w) and hydrochloric acid (HCl; 30%, w/w) were acquired as suprapur® reagents from Merck (Darmstadt, Germany). Hydrogen peroxide (30%, w/v) and ethanol (95%, v/v) were obtained from Merck. The working solutions of Ni (1 mg L^{-1}) and Co (0.1 mg L^{-1}) were obtained by diluting the 1 g L^{-1} reference standard in 0.01 mol L^{-1} HNO$_3$. A 2 mol L^{-1} ammonium buffer (pH 9.5) was prepared by mixing 112.5 mL of concentrated ammonia solution (25% w/w) with

181 53 mL of HCl (30% w/w) and filled up to 500 mL with Milli-Q purified water. 0.1 mol L^{-1}

182 dimethylglyoxime stock solution was prepared in ethanol (95%, v/v).

183   For SeaFAST preconcentration, ammonium acetate buffer (pH 8.5±0.05) was prepared

184 by mixing 300 mL of concentrated NH_3 (20-22%) with 180 mL acetic acid (>99%) and filling

185 to 1 L with Milli-Q water. Concentrated NH_3 and acetic acid were acquired as UpA grade

186 reagents from Romil (Cambridge, UK). The SeaFAST elution acid was prepared with 1 mol L^{-1}

187 sub-boiled HNO_3 and 1 µg L^{-1} Indium (In) in Milli-Q water. Rinse acid for the SeaFAST and

188 ICP-MS was prepared with 1 mol L^{-1} HNO_3 (65-67%) in Milli-Q water. The HNO_3 used for

189 elution acid was sub-boiled in-house, while the HNO_3 used for rinses, which had lower purity

190 requirements, was SpA grade and not sub-boiled. Stock solutions of Ni (2 mg L^{-1}) and Co (0.6

191 mg L^{-1}) were prepared from a 1000 mg L^{-1} standard in 1 mol L^{-1} HNO_3 (sub-boiled) for storage,

192 and further diluted in 1:100 Milli-Q water shortly before analysis. For quality control, seawater

193 certified reference materials (CRMs) CASS 6 and NASS 7 were obtained from the National

194 Research Council Canada (NRC-CNRC).

195

196 *2.3 Collection of samples and study area*

197

198   All procedures related to the collection and analysis of trace element samples were

199 carried out according to the GEOTRACES cookbook (Cutter et al, 2017;

200 https://geotracesold.sedoo.fr/images/Cookbook.pdf). The GEOTRACES process study cruise

201 M147 (Amazon – GEOTRACES, GApr11) took place in April-May 2018 during a period of

202 high river discharge as described elsewhere (Koschinsky et al., 2018; Zhang et al., 2020;

203 Hollister et al., 2021). Surface water samples were collected with a towed-fish sampling device

204 from a full range of salinity gradients (0 to >35) in the Amazon and Pará River estuaries and

205 associated mixing region (Figure 1). During the cruise, samples from the towed-fish were

206 pumped into the trace element clean laboratory container using a Teflon diaphragm pump and

207 a braided polyvinyl chloride (PVC) tube. The towed-fish sampling device was positioned at ~

208 2 to 3 m water depth. Water column samples were collected with an ultra-clean conductivity-

209 temperature-depth device (TM-CTD, Seabird 911plus) equipped with a water sampling rosette

210 (Seabird 32) and 24 contaminant-free water sampling bottles (C-Free, Ocean Test Equipment)

211 was used for collecting samples at different depths (~10–2000 m). A specialized winch with a

212 plastic-coated cable were used to operate the TM-CTD. After recovery, the TM-CTD bottles

213 were immediately carried to the trace element clean sampling container. All sample bottles were

low density polyethylene (LDPE, Nalgene) and acid washed prior to use. Samples for determination of labile particulate trace element concentrations were collected directly (i.e. without filtration) from the sampling device. Samples were filtered in-line through a 0.8/0.2 μm cartridge filter (AcroPak1000™) into acid washed low-density polyethylene (LDPE) bottles. The samples were filtered shipboard in the clean laboratory container through 0.2 μm membranes to obtain the dissolved fraction and further filtered through Anapore 0.015 μm filters to obtain the soluble fraction. The large colloidal fraction was operationally-defined as the difference between the dissolved and soluble fractions (0.015 μm < colloidal < 0.2 μm). Ultrafiltration at <1 and <10 kDa was also performed at four selected stations (three at the Amazon North transect and one at the mangrove area) from the towed-fish with a Merck Millipore Cross Flow system (for details, see Koschinsky, 2018). The four surface water samples were chosen as representatives of the Amazon river endmember (15), a sample of intermediate salinity along the mixing transect (98), a seawater endmember (25) and a representative of the mangrove belt (36) (Figure 1B). Two- and five-liter water samples were taken from the towed-fish to perform 1kDa and 10kDa ultrafiltration to determine the distribution of trace metals in the different size fractions. After each sample, 30 mM ultrapure HCl (34%, Roth) was circulated for 10 minutes to remove any remaining colloids from the system. For Ni and Co analysis, only the permeate of the ultrafiltration process was available.

All the samples were acidified on board to pH ~1.8 using 0.024 mol L^{-1} HCl (Fisher, ultra) and stored at room temperature until the shipboard measurements by AdCSV were performed. Afterwards, the samples were stored at 4 °C. A special trace element conductivity-temperature-depth device (TM-CTD) equipped with a water sampling rosette (GEOMAR Helmholtz Centre for Oceanographic Research, Kiel, Germany) equipped with 24 contaminant-free water sampling bottles (C-Free, Ocean Test Equipment) was used for collecting samples at different depths (~10–2000 m). A specialized winch and plastic-coated cable (GEOMAR) were used to operate the TM-CTD. After recovery, the TM-CTD bottles were immediately carried to the trace element clean sampling container.

The samples presented in the study area, which included the Amazon and Pará River estuaries and surrounding Northwest Brazilian Continental Shelf, were grouped for analysis based on salinity and source (Figure 1B). The Amazon River transect encompassed the Amazon River outflow region and a wide range of salinities (S ~ 0.3–35). To the south, the Pará River transect encompassed a similar salinity range (S ~ 0.4–28) but has a distinct river catchment area. The Pará is sourced largely by the Tocantins River to the south (not shown), which flows through the state of Tocantins and is defined by a drier climate and heavier anthropogenic

disruption compared to the Amazon River basin. Upon estuarine mixing, the waters from both source rivers converge to form a plume of intermediate salinity (S ~ 10–26) that ages as it flows north (hereby referred to as "Plume North"). To the south of the Pará River, mangrove forests along the coast contribute groundwater and organic matter (Dittmar and Lara, 2001). Samples collected parallel to this region (referred to as the "Mangrove Belt") generally showed decreased salinity relative to the open ocean (S ~ 28–35). The North Brazil Current ("NBC") flows northwest from the South Equatorial Current along the coast of northern Brazil and defines the seawater endmember (S ⩾ 35). Because the NBC pushes the freshwater input from the Mangrove Belt north towards the plumes from the Pará and Amazon Rivers, the freshwater signal moving northwest along the Brazilian coast contained characteristics of the mangrove forest, freshwater from two major rivers, and interactions with surface sediment on the Amazon shelf.

2.4 Stripping voltammetric measurements

Direct determinations of Ni and Co were carried out shipboard by adsorptive cathodic stripping voltammetry (AdCSV) in all the 0.2 μm filtered samples to quantify the electrochemically active forms of Co and Ni, which naturally exist as labile complexes or hydrated ions (labile dissolved fraction). Labile dissolved concentrations were determined directly after reagents had been added and the sample purged (i.e ca. 6 min after reagent addition). Additional analysis in the home laboratory was performed to determine labile particulate (unfiltered aliquot) and total dissolved (<0.2 μm filtered aliquot) trace elements after UV irradiation for 4 h. Concentrations of labile particulate Ni and Co were obtained by subtracting the concentration in the total dissolved fraction (<0.2 μm) from concentrations in the unfiltered, acidified fraction; percentages of labile particulate metals are expressed relative to total unfiltered concentrations.

Prior to UV digestion of the samples, 10 mL of each sample was transferred to a quartz tube, and 30 μL of H_2O_2 30% (v/v) was added. The samples were then UV-irradiated for a total of 4 h at 88 ± 2º C, and the addition of H_2O_2 30% (v/v) was repeated after 1h, 2h, and 3h of irradiation. After the irradiation process, the samples were cooled to room temperature prior to AdCSV determination of Ni and Co as described above.

In the AdCSV measurements, 500 μL ammonium buffer (final pH = 9.0 ± 0.2) and 50 μL of 0.1 mol L^{-1} DMG was added to 10 mL of water sample (final concentration 50 μmol L^{-1}). The solution was then deaerated with nitrogen for 5 min. A deposition step of 90 s at –0.60

V was applied by stirring at 2000 rpm, followed by a 15 s resting period. Afterwards, the voltammograms were recorded between −0.60 and −1.20 V in the differential pulse mode with a pulse amplitude of −50 mV, a pulse duration of 40 ms and a scan rate of 10 mV s^{-1}. Cobalt and Ni were quantified simultaneously by the standard addition method (n = 3). Standard addition calibration curves were obtained in each sample after the repeated addition (three times) of 8.50 nmol L^{-1} Ni and 0.85 nmol L^{-1} Co. The peaks were found at –0.95 V for Ni^{2+} and –1.10 V for Co^{2+}.

The accuracy of the AdCSV measurements was evaluated by determining the concentration of total Ni and Co in a freshwater NIST (National Institute of Standards and Technology, USA) 1640a certified sample. The certified sample was UV digested in triplicate following the procedure described above, after which the Ni and Co concentration were determined by repeated addition (three times) of 8.50 nmol L^{-1} Ni and 1.70 nmol L^{-1} Co in the samples diluted (100-fold) in the voltammetric cell (Table 1 Supplemental). The analytical error was determined from repeated measurements of the NIST 1640a certified sample and CTD samples (n = 10) to be 10.32% for Ni and 11.13% for Co. The detection limits for Ni (=0.25 nmol L^{-1}) and Co (=0.010 nmol L^{-1}) were defined as three times the standard deviation of six determinations of blank measurements carried out onboard ship. Average blank values were determined to be 0.64 nmol L^{-1} for Ni and 0.017 nmol L^{-1} for Co by AdCSV.

2.5 SeaFAST preconcentration and ICP-MS analysis

Trace elements were preconcentrated and analyzed by inductively coupled plasma-mass spectrometry (ICP-MS) at GEOMAR Helmholtz Centre for Oceanographic Research (Kiel). Ni and Co were quantified using isotope dilution and standard addition, respectively, as described by Rapp et al (2017). Samples were preconcentrated on a chelating resin (Wako or Nobias) using an automated SeaFAST system (ESI SeaFAST-Pico^{TM}) in order of increasing salinity, with the exception of the lowest salinity samples (S < 2), which were analyzed without preconcentration. Prior to preconcentration, samples that had been acidified shipboard (pH ~1.8) were spiked with a Ni isotope standard that contained known ratios of ^{60}Ni and ^{62}Ni. Co has only one stable isotope and therefore was quantified by standard addition. A 5 point calibration curve (0–1.3 nmol L^{-1} Co) was prepared in mixed sample seawater to match the matrix of the samples and was run at the beginning and end of each SeaFAST. In addition, a smaller 3 point curve was run once per every 10 samples to account for any drift. Each SeaFAST sample run was also accompanied by several manifold (air) blanks, as well as quality control

316 (QC) South Atlantic seawater and the certified reference materials (CRMs) NASS-7 and CASS-

317 6.

318   Samples, QCs and CRMs were all UV-irradiated for 4 h prior to preconcentration in

319 order to ensure complete recovery of the total dissolved fractions (Milne et al. 2010; Biller and

320 Bruland 2012). During the preconcentration, the sample was buffered in-line with ammonium

321 acetate (pH 8.5 ± 0.05) to a final pH of 6.2 ± 0.05 and loaded onto the chelating column. The

322 column was then rinsed with Milli-Q water and flushed with an elution acid solution of 1 mol

323 L^{-1} HNO_3 with 1 µg L^{-1} of In as an internal standard. Trace elements were eluted with the acid

324 at a 25-fold preconcentration factor. Between samples, the column was rinsed in 1 mol L^{-1}

325 HNO_3. After preconcentration, counts for ^{59}Co, ^{60}Ni, ^{62}Ni and ^{115}In were measured on a Thermo

326 Element XR ICP-MS. Counts were normalized to In and quantified using the isotope spikes

327 (for Ni) and standard addition curves (for Co).

328   Our measured values were in good agreement with the CRMs (Table 1 Supplemental).

329 The analytical error was determined using the Nordtest method (see Rapp et al., 2017) based

330 on NASS-7 and CASS-6 measurements to be 7.3% for Ni and 9.7% for Co. Average manifold

331 blank values, which accounted for SeaFAST preconcentration and ICP-MS measurement, were

332 0.14 nmol L^{-1} for Ni and 0.46 pmol L^{-1} for Co.

333

3. Results and Discussion

3.1 Stripping voltammetric analysis detected a dominant reactive Ni fraction but an absence of reactive Co

In natural water systems, Co(II), and to a lesser extent Ni(II), are bound to organic ligands, which comprise a portion of the total dissolved organic matter (DOM) pool. In addition, Ni(II) and Co(II) ions can be scavenged to larger particles formed from flocculating inorganic or organic colloids. Furthermore, Ni(II) and Co(II) can be also present partially as free ions or inorganic complexes in seawater (Cosovic et al., 1982; Motekaitis and Martell, 1987; Byrne et al., 1988). Given the relative high stability constant of Ni-DMG and Co-DMG complexes, Ni(II) and Co(II) can be partially displaced from natural DOM when excess DMG is added as a complexing agent to natural waters, and the extent of this displacement depends on the conditional stability constants (log K) of the natural organic ligands. This displacement of Ni and Co explains the appearance of voltammetric signals for Ni(II) and Co(II) in natural water samples, even without prior UV digestion of the organic matter (Van den Berg and Nimmo, M., 1987; Donat et. al, 1994; Saito and Moffett, 2001; Xue et. al, 2001). In these cases, the measured Ni or Co concentration is defined as the labile or "reactive" species (Sander and Koschinsky, 2000), which reacts with the electrode surface as a free hydrated ion or an electroactive organic complex. Our shipboard measurements of reactive Ni and Co species were performed using stripping voltammetric (SV) analysis in the presence of DOM, which can be understood by reaction mechanisms reported by Saito and Moffett (2001). The electrochemical reduction of the DMG complexes involving the exchange of $10e^-$ allows for high sensitivity in voltammetric determination of Ni and Co (pmol L^{-1} to nmol L^{-1} levels) (Saito and Moffett, 2001).

DMG complexes have log K values determined by independent methods in the range 17.20–18.84 for Ni(DMG)$_2$ (Dyrssen et al., 1959; van den Berg and Nimmo, 1987; Martell and Smith, 1989) and 11.50–12.85 for Co(DMG)$_2$ (Zhang et. al, 1990; Saito and Moffett, 2001). A higher intrinsic stability constant of 22.92 for Ni (DMG)$_2$ was also reported by Xue et al. (2001). Considering the reported log K for Ni(DMG)$_2$ and Co(DMG)$_2$ as well as the excess concentration of ligand added to the samples, DMG can be expected to displace Ni from organic ligands with lower reaction coefficients (α_{ML}) in estuarine waters (Nimmo et al., 1989). In all shipboard samples of untreated estuarine water after the DMG addition, we observed voltammetric signals for reactive Ni species at –0.95 V but not for reactive Co species at –1.10

V. The observed Ni(DMG)$_2$ signals were consistent with a previous study that reported naturally-occurring Ni-organic complexes in freshwater and marine systems with stability constants in the range of log $K \sim$ 12-17 (Doig and Liber, 2007). On the other hand, the absence of SV signals for Co(DMG)$_2$ in the same samples can be attributed to the presence of relatively strong organic complexes of Co with natural ligands. These observations are supported by a previous study (Saito and Moffett, 2001), which suggested that Co(II) may be strongly complexed with natural organic ligands in seawater (log $K \sim$ 14-18). Thus, much higher reaction coefficients of Co with natural organic ligands (α_{CoL}) in relation to DMG may explain the non-lability observed for dissolved Co in our samples. In addition, the apparent absence of reactive Co may also be related to the presence of kinetically inert Co(III) complexes with DOM (Duckworth et al., 2009; Ellwood and van den Berg, 2001.

A third possibility for the lack of Co(DGM)$_2$ signal is the slow reaction kinetics of Co(II) when compared to Ni(II), even in the presence of excess DMG (Saito and Moffett, 2001; van den Berg and Nimmo, 1987; Xue et al., 2001). Since the time allowed for equilibration of the samples prior to shipboard measurement of the stripping current was relatively short (< 6 min), it could partly explain the apparent absence of labile Co. In order to investigate this possibility, we measured surface water samples of low and high salinities after 12 h and 24 h following the addition of 50 μmol L^{-1} DMG; however, the resulting signals for the Co–DMG complex at −1.10 V were deformed and unusable for quantitative analysis, possibly due to the interference of surface-active compounds from DOM on the electrode surface. Only after the UV digestion of the samples, could signal could be detected and total dissolved Co determined in the absence of interfering organic ligands (Figure 1 Supplemental).

3.2 Non-conservative behavior was observed for total dissolved Ni and Co

Reactive Ni and total dissolved Ni and Co obtained by voltammetry (AdCSV) were comparable to total dissolved Ni and Co obtained by ICP-MS (Figure 2). ICP-MS measurements, following UV-digestion and preconcentration of trace metals, yielded Ni concentrations in the same range ($\sim$2–10 nmol L^{-1}) as the AdCSV measurements of the same samples (Figure 2 A-C). AdCSV analyses of total dissolved Ni compared to reactive dissolved Ni showed slightly higher concentrations and a more disperse distribution for total dissolved Ni (Figure 2 Supplemental). However, the similar trends between total and reactive Ni indicate that the majority of dissolved Ni species are present as relatively labile complexes or Ni^{2+} free ions. This result is consistent with previously reported behavior for Ni in seawater, wherein a

relatively small fraction of Ni is expected to be complexed by strong organic ligands (van den Berg and Nimmo, 1987; Boiteau et al., 2016).

Comparative measurements of total dissolved Co performed by ICP-MS and AdCSV in the home laboratories resulted in similar concentrations ($\sim$0.1–1.5 nmol L^{-1}) for most samples along the salinity gradient (Figure 2 D-F). Unlike for Ni, reactive Co species were not detected in our dissolved samples, consistent with a predominance of strong Co-DOM complexes (Bown et al., 2012). The difference observed for AdCSV and ICP-MS measurements may be attributed to differences in calibration methods or the final detection methods (Figure 3 Supplemental). According to Oldham et al. (2017), the precipitation of humic matter may be associated to the loss of Fe/Mn ligand complexes to bottle walls before seawater is submitted to UV digestion. It could be also associated to the discrepancies observed here for Co by AdCSV and ICP-MS.

In a study of the Amazon estuary and plume from 1976, a conservative Ni distribution was observed (6.3 to 1.5 nmol kg^{-1}; Boyle et al., 1982). Our study showed a similar distribution, but slightly higher concentration ranges mainly at low salinity regions (Figure 4 Supplemental). On the other hand, dissolved Cu measured from this same research cruise (Hollister et al., 2021) showed no change in concentration compared to Boyle et al. (1982), indicating that this concentration increase cannot be solely attributed by a change in river dynamics. Instead, the higher Ni may be related to anthropogenic activities, including possible increased Ni mining in the Amazon River catchment area (Melfi et al., 1988; de Oliveira, S.M.B. et al., 1992).

Distinct influences from the Amazon and Pará rivers as natural sources of Ni and Co to the estuary were observed for both ICP-MS (Figure 3 A, B) and voltammetric (Figure 3 C, D) data, where dissolved Ni and Co were higher in the Pará River outflow area (Figure 2 A–F). River endmember values for Ni were determined at S = 0.35 (Pará Transect) and S = 0.18 (Amazon Transect) to 9.18 and 5.93 nmol L^{-1}, respectively. For Co, river endmember values were determined as 2.29 nmol L^{-1} (Pará Transect) and 2.01 nmol L^{-1} (Amazon Transect). At higher salinities (S $\geq$ 15), the Amazon and Pará River transects became indistinguishable, indicating that thorough mixing likely occurred. In future studies, the sources of Ni could be further refined by conducting isotopes studies, due to the different isotope signatures of Ni from the Amazon tributaries and oceanic endmembers (Revels et al 2021).

Reactive dissolved Ni, total dissolved Ni and total dissolved Co species all decreased with increasing salinity, although some non-conservative behavior was also observed (Figure 2). A mid-salinity local minimum (S $\sim$13–25) was observed for reactive dissolved Ni which may be attributed to possible biological uptake, particle adsorption and/or colloidal flocculation. Large colloidal Ni was primarily observed in the low-mid salinity range (S <13.9; section 3.4),

supporting the idea of colloidal flocculation at higher salinities. Bioproductivity was higher in this salinity range compared to lower and higher salinity regions, reflected in elevated chlorophyll *a* data (Hollister et al., 2021). Furthermore, bacterial Mn oxidation might be higher in higher productivity regions (Sunda and Huntsman, 1987), so scavenging rates of Co could be higher here. The increase in concentrations of dissolved Ni and Co following the local minima in the mid-salinity region (S $\geqslant$ 16) may reflect desorption from particles (Morris et al., 1965; Coleman, 1966).

The slightly elevated levels of dissolved Ni and Co species in the Mangrove Belt samples (S ~ 28-35), compared to samples of equivalent salinities in the Amazon and Pará transects (Figure 2) suggest an additional source of trace element-rich groundwater inflow from this region (Thanh-Nhoab et al., 2018; Sadat-Noori and Glamore, 2019). Mangrove forests in Northern Brazil are areas of high productivity and act as natural sources of DOM and particulate matter to the Atlantic Ocean (Dittmar et al, 2006; Tremblay et al, 2007). Ni and Co can be transported through particulate materials (especially Co, which is subject to particle-scavenging) and dissolved organic complexes from the mangrove coastal zone. Upon mixing of groundwater and seawater, desorption of trace metals may occur, resulting in the concentration increase observed in the mid-high salinity range of the Mangrove Belt samples (Figure 2). This supports previous findings indicating that the adjacent mangroves play an important role for not only the aquatic carbon budgets (Dittmar et. al, 2001), but also for concentrations of trace elements and associated organic matter in the Northwest Brazilian continental shelf (Hollister et al, 2021).

3.3 Depth profiles indicate effects of scavenging, biological interaction, and Antarctic Intermediate Water intrusion

Biological uptake and regeneration have a strong influence on the distribution of metals throughout the water column in estuaries and the open ocean (Smoak et. al, 2006; Boyd et al., 2017; Archer et. al, 2020). To study the processes governing dissolved Ni and Co at depth, TM-CTD samples (0-2000 m) were analyzed (Figures 4 and 5). Concentrations in the upper water column ($\leqslant$ 25 m) were highest in station 9 (Figure 1C), which was lowest in salinity and nearest to the Pará River source. In all stations, the partial depletion of Ni in surface waters was consistent with its well-known nutrient-like behavior (Sclater et al. 1976, Bruland et al. 1980) and with a recent study in South Atlantic waters (Archer et al. 2020). Our dissolved Ni minimum at 30-60 m (~1 and 3 nmol L^{-1}) may be attributed to similar removal mechanisms (e.g.,

biological uptake and/or particle adsorption) as that observed in dissolved Ni in mid-salinity surface samples (S ~13–25). Moreover, the close agreement of the results for reactive and total dissolved Ni (Figure 4C, 5C) may indicate that most of the Ni participating in the processes of biological uptake at the surface and subsequent regeneration at depth is present in the reactive form. The Ni concentration increase at 500-1000 m (Figure 4 A-B) indicates possible regeneration or the presence of Antarctic Intermediate Water (AIW) masses (Hawco et al. 2018). Co also displayed nutrient-like increase at similar depths to Ni (Figure 4D-E), consistent with data from Saito and Moffett (2001).

In addition to nutrient uptake and regeneration, the decrease in surface Co (Figure 5D-E) and possibly Ni in the upper ~50 m (Figure 5A-C) may indicate particle-scavenging behavior. The apparent combination of scavenging and biogenic uptake and regeneration for Co is consistent with other GEOTRACES studies throughout the global oceans (see e.g. Hawko et al. 2018 and references therein). In addition to its role as a micronutrient, Co may be scavenged to particles such as Mn-oxides in the water column (Tebo et al. 1984; Lee and Fisher 1993). More limited studies indicate that Ni can also be subject to particle scavenging (Balistrieri and Murray 1986; Tani et al. 2004), and a recent seawater regeneration experiment indicated that Ni and Co concentrations in the water column are likely influenced by a combination of particle scavenging, biogenic uptake and regeneration (Hollister et al, 2020). Thus, biological and particle scavenging processes likely both influence the cycling of Co and Ni in this estuary environment, which is rich in both particulate matter (section 3.4) and biogenic activity.

3.4 Labile particulate (>0.2 μm) Co and Ni and large colloidal Co are present throughout the estuary

The degree of sorption and desorption of metals on and from particles is an important driver of their fate and transport in estuaries (Mosley and Liss, 2020) and the bioavailability of these metals in the estuarine mixing zone. Labile particulate Ni and Co (i.e. the >0.2 μm fraction leachable by acidification and UV digestion) were detected throughout the full salinity range of the sample area (Figures 6 A-B). The highest labile particulate Ni and Co concentrations were detected in the Amazon transect and decreased with respect to salinity. Labile particulate Ni and Co in the Amazon River end member comprised 69% and 83% of the total measured concentrations, respectively (Figure 6 C-D). Our Ni concentrations are similar to a recent study

by Revels et al. (2021), which found a dissolved load of 0.25-0.70 times that of the labile particulate material concntrations in the Amazon River. The relative distribution of Ni and Co as labile particulate species indicates that both elements enter the estuarine mixing zone bound primarily to particles derived from the Amazon River, due to the comparatively higher water volume and associated particle flux compared to that of the Pará River (Figure 6 A-D). The Amazon, Pará and Plume North transects were indistinguishable from each other at S $\geq$ 10, indicating thorough early mixing. In addition to riverine contributions, brackish groundwater from the Mangrove Belt also appeared to be an important source of labile particulate Ni and Co, resulting in a slight increase in both metals observed in mangrove-associated samples (S > 28; Figure 6 A-D). Size fractionation is known to affect isotopic fractionation of Ni in the Amazon river, with lighter Ni preferentially partitioned to the particulate phase (Revels et al, 2021). Thus, our data could be used to support future isotopic studies to investigate sources and sinks of Ni in the Amazon Estuary and ocean.

Ni and Co concentrations in the large colloidal fraction were determined by subtracting the soluble fraction (<0.015 μm) from the dissolved fraction (<0.2 μm), and the subsequent colloidal error was calculated from propagation. Paired t-tests between the dissolved and soluble fractions showed a significant difference between the two fractions for Co ($p<0.05$, n=75) but not for Ni, indicating that large colloidal species (0.015 – 0.2 μm) played a more important role for Co (Figure 7). For all except a few low salinity samples, the soluble and dissolved fractions for Ni (Figure 2A-B) were within error of each other, and no significant colloidal fraction was detected (Figure 7 A-B). While colloidal Ni was only detected in the coastal regions of Amazon and Pará rivers, colloidal Co was present throughout the estuary, with contributions from the Amazon and Pará rivers as well as the Mangrove belt (Figure 7 C-D). Colloidal Co, expressed both as concentrations and as percentage of total dissolved, was highest in the low-mid salinity range of S ~3-6 for the Amazon transect (up to 0.28 nmol L-1 and 59% of total) and S ~7 for the Pará transect (1.6 nmol L-1, 86% of total). This low-salinity colloidal maximum for Co may be related to the mixing of seawater with the Amazon River water in the northern region of the plume and disaggregation of particulate matter, which has been observed for uranium in other areas of the Amazon estuary (Swarzensky and Booth, 1995). The colloidal fraction of Co generally decreased from S ~ 7 (86%) to S ~ 22 (16%), consistent with studies conducted for other metals in the Amazon, wherein a drawdown in trace elements resulted from a combination of coagulation of river colloids and particle scavenging (Boyle et al., 1977; Sholkovitz and Price, 1980; Swarzensky and Booth, 1995). At higher salinities, the

colloidal fraction of Co increased slightly, primarily in the Mangrove Belt samples (up to 33%), possibly reflecting an influx of brackish groundwater containing elevated organic matter.

3.5 A fraction of Ni is truly dissolved

We performed an additional ultrafiltration (<10 kDa and <1 kDa) analysis on four samples of varying salinities throughout the study area (Figure 1B). Ultrafiltration, which separates fractions based on weight rather than diameter, is not directly comparable to standard membrane filtration. However, a weight of 1-10 kDa corresponds to a pore diameter of roughly 2.8-4.4 nm (Sarbolouki, et al 1982), so both ultrafiltered fractions can be expected to have lower concentrations than the dissolved and soluble fractions. Cobalt had no discernible trends among size fractions, indicating possible contamination during filtration and data are not presented here. Nickel concentrations generally decreased with decreasing filter size and displayed similar trends between ICP-MS and AdCSV analyses (Figure 8). The corresponding dissolved and soluble Ni samples were within error of each other, corroborating the other sample results (Figure 2 A-B). With the exception of the AdCSV results for sample 98 (<10 kDa), the ultrafiltered fractions were measurably lower than the soluble and dissolved fractions. In stations 15, 25 and 36 the <1 kDa fraction was lower in concentration than the <10 kDa fraction for the respective analyses; for station 25 AdCSV analysis, both fractions were below detection (<0.25 nmo L^{-1}). As observed for the other dissolved and soluble samples (Figure 2), Ni concentrations decreased with increasing salinity, and all size fractions were lowest in concentration in the seawater end member (station 25). The highest concentration of <10 kDa Ni was observed in sample 36, (Mangrove Belt, S = 29), possibly indicating a unique geochemical environment for this region, which is defined by groundwater discharge, high DOM concentrations and elevated biological activity. Our ultrafiltration data indicate that an important portion of soluble Ni is transported from the Amazon river and mangrove belt to the ocean in a truly dissolved form of <10 kDa or even <1kDa and can contribute to the biogeochemical cycling of Ni in the oceanic water column.

4. Conclusions

We present a comprehensive speciation study of Ni and Co in the Amazon and Pará River estuaries, mixing zone and surrounding regions of the Northwest Brazilian Continental

shelf. Ni and Co concentrations were quantified in surface water and depth samples using comparative analyses by voltammetry (AdCSV) and mass spectrometry (SeaFAST preconcentration and ICP-MS analysis). AdCSV analyses indicated that, in relation to DMG-metal complexes, Ni is governed by relatively weaker organic or inorganic complexes or Ni^{2+}, while Co is governed by relatively stronger organic complexes. In addition, the high fraction of reactive Ni compared to total dissolved suggested high bioavailability. This similarity between reactive and total dissolved Ni was highlighted in both surface samples and in nutrient-like depth profiles. Dissolved Ni and Co from CTD profiles (~10-2000 m water depth) showed a nutrient-like increase at depth (~500-1000 m), with likely additional influence of the Antarctic Intermediate Water (AIW) for Ni. Our data may support studies investigating the sink-source relationships of Ni isotopes in the ocean (e.g., Revels et al., 2021), as particulate phase Ni isotopes are uniformly much lighter than the dissolved phase Ni isotopes, and hence, Ni partitioning between different size fractions plays an important role for Ni isotopic fluxes in an estuarine system.

Throughout the estuary, the distributions of Ni and Co were governed by a combination of input and removal mechanisms. Concentrations of Ni and Co in dissolved, soluble and, for Ni, truly dissolved (<10 and <1 kDa) surface water samples correlated negatively with salinity. Deviations from conservative river-seawater mixing behavior were attributed to possible particle adsorption-desorption, colloidal flocculation, biological activity and additional input from sources such as mangrove-derived groundwater. Ni and Co species entered the estuarine zone from the Amazon and Pará Rivers predominantly associated with particles (>69% of total for river end members). Large colloidal species (0.015–0.2 μm) of Ni and Co were observed in the mixing zone, but were only detectable at low salinities for Ni. For both metals, dissolved species were transported in the estuarine mixing zone primarily as soluble species (<0.015 μm). However, elevated concentrations of colloids at low salinity may provide a removal mechanism for dissolved Ni and Co via colloidal flocculation upon seawater mixing. The Mangrove Belt also played an important role in contributing to both dissolved (<0.2 μm) and particulate-bound dissolvable (>0.2 μm) species of Ni and Co. Elevated levels of Ni and Co in this region were attributed to a possible influx of groundwater and/or desorption process from particulate material.

The Amazon basin has increasingly been subject to anthropogenic impacts. Prior to this study however, no recent Ni or Co data existed for the Amazon estuary and surrounding Northwest Brazilian Continental Shelf. This study established concentration levels and salinity

distributions of Co and Ni at high resolution. The data presented here will therefore be essential for evaluating future changes in trace elements in this region.
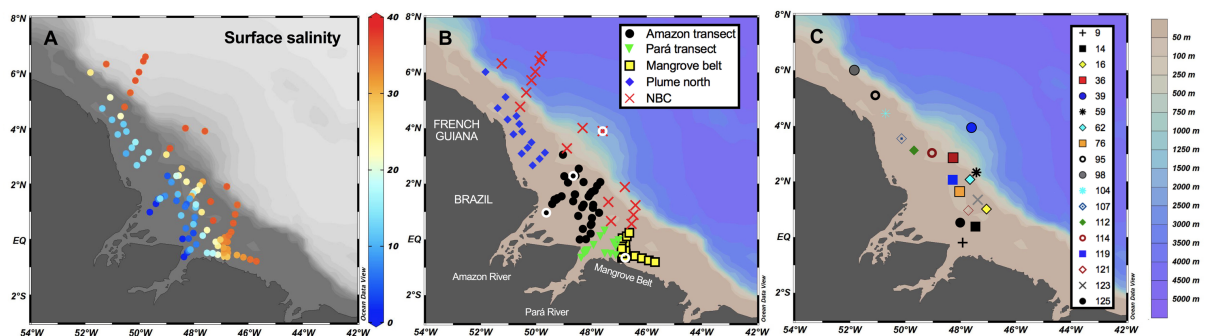
Acknowledgements

Figures


Figure 1: Transects and salinity gradient of Amazon and Pará River estuaries, mixing plume and nearby regions of the Northwest Brazilian Continental Shelf obtained during the research cruise M147, Amazon – GEOTRACES GApr11: (**A**) surface salinities of towed-fish samples (**B**) towed-fish samples, grouped according to source and region and (**C**) locations of TM-CTD depth profiles analyzed in this study. The white circles in B represent locations where the samples for ultrafiltration were collected.
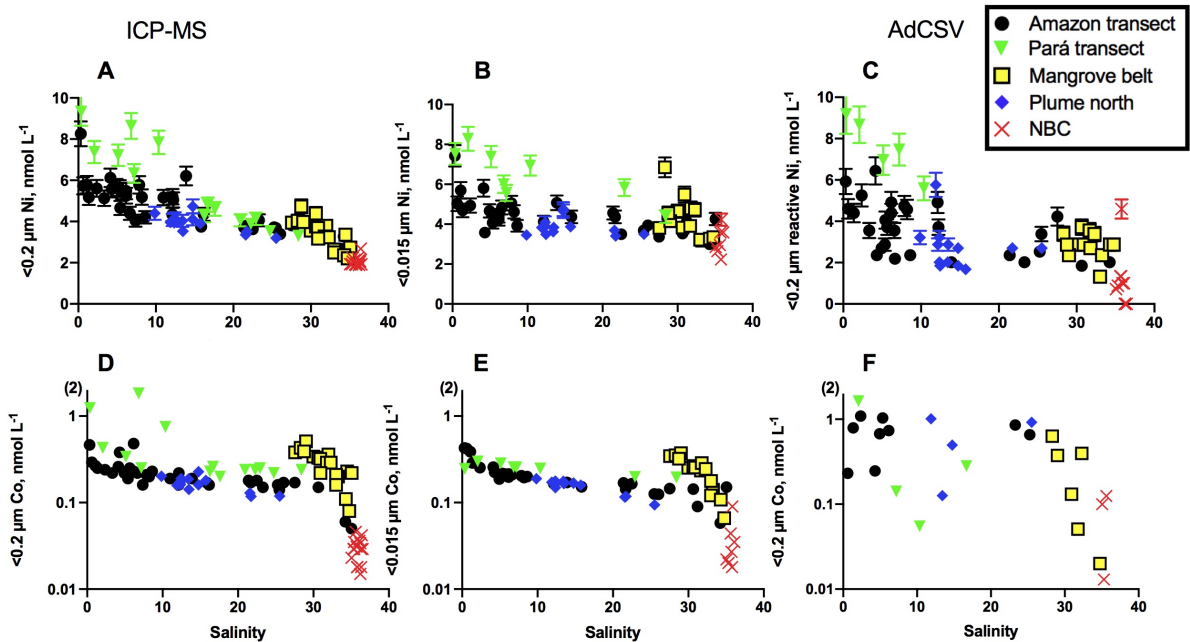
Figure 2: Comparative distribution of total dissolved (<0.2 μm) and soluble (<0.015 μm) Ni (**A-B**) and Co (**D-E**) by ICP-MS methods, reactive dissolved Ni (**C**) by AdCSV methods and total dissolved Co (**F**) by AdCSV methods in the study area.
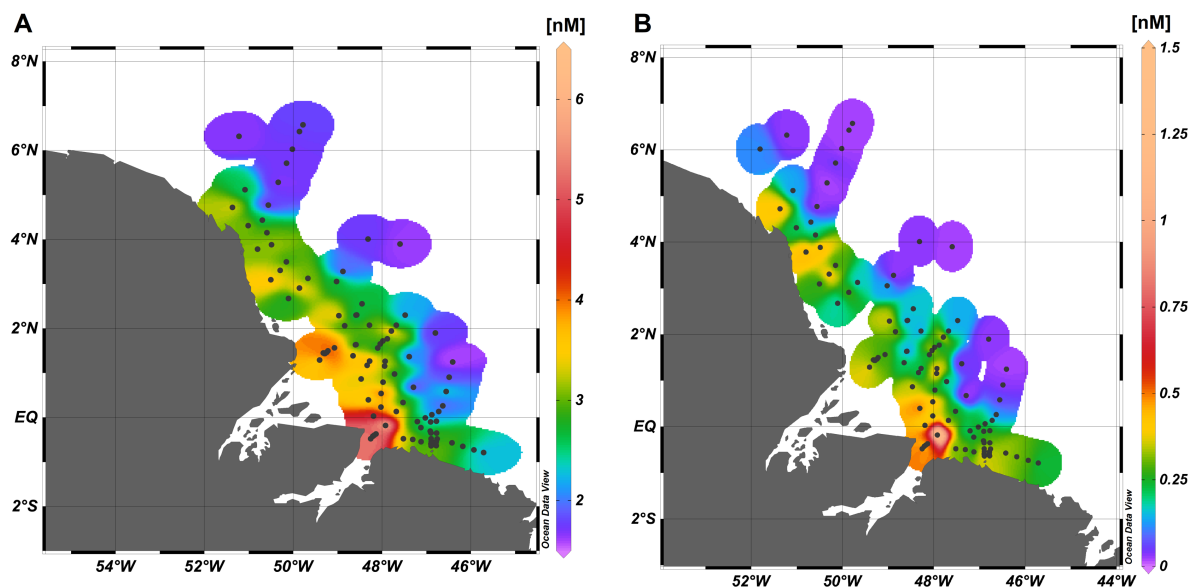
Figure 3: Spatial distribution of total dissolved Ni and total dissolved Co in the study area measured by ICP-MS (A, B) and AdCSV (C, D).

632
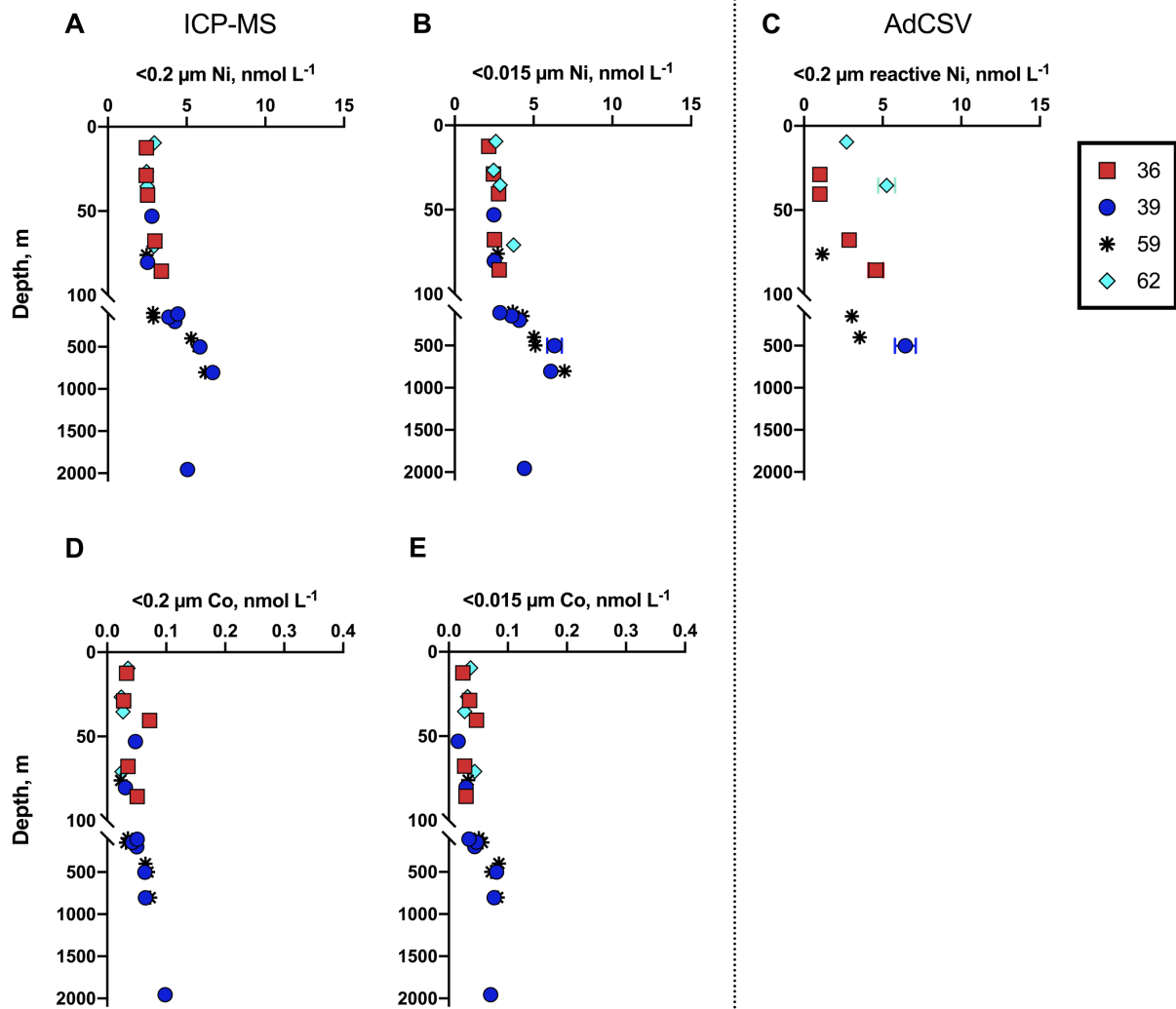
Figure 4: Depth profiles of dissolved (<0.2 µm) and soluble (<0.015 µm) Ni and Co species
measured by ICP-MS in samples collected from CTD bottles in the study area (high salinity).

635
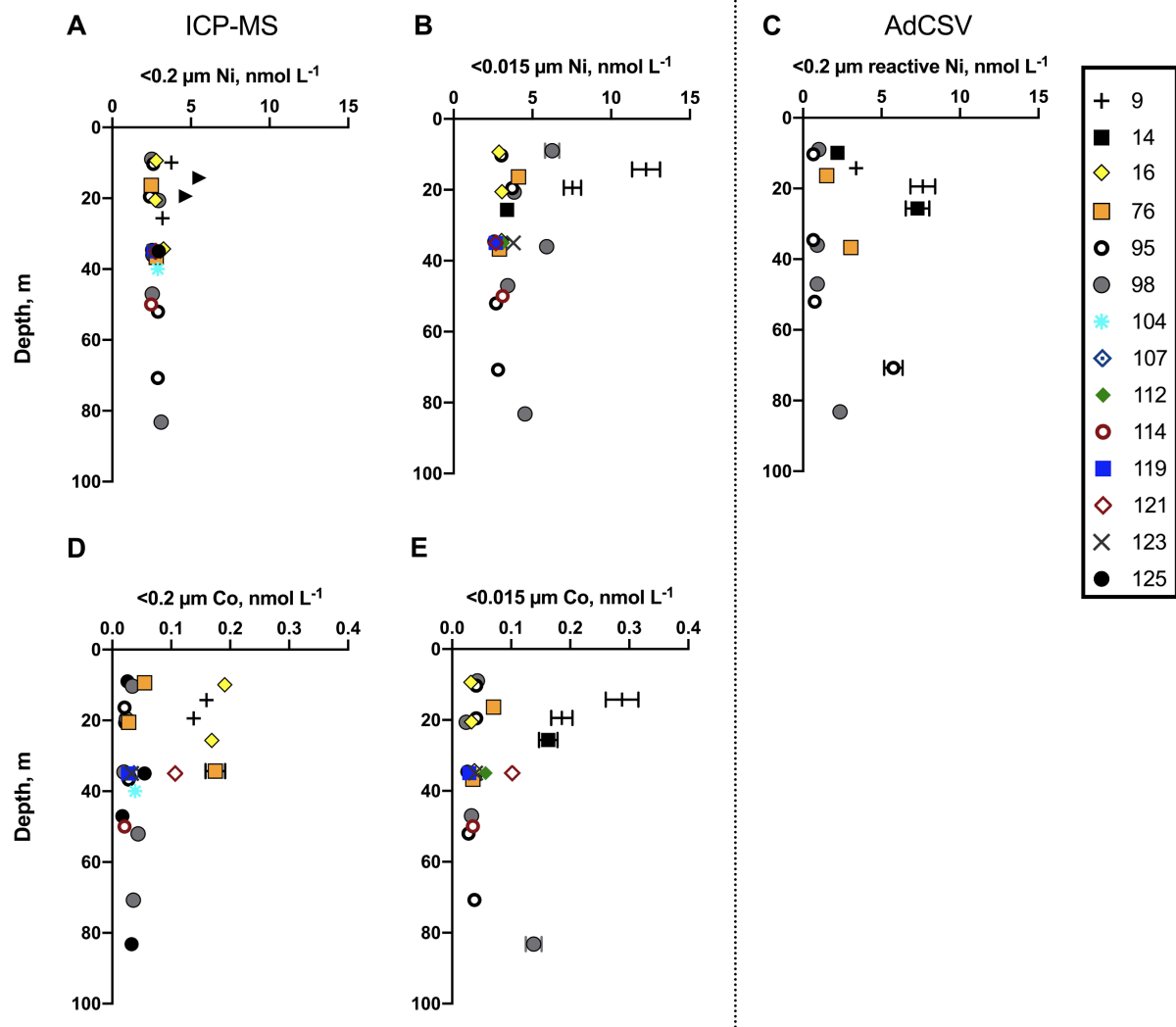
Figure 5: Depth profiles of dissolved (<0.2 µm) and soluble (<0.015 µm) Ni and Co species measured by ICP-MS in samples collected from CTD bottles in the study area (low salinity). The symbols correspond to locations of CTD casts as specified in Figure 1C.
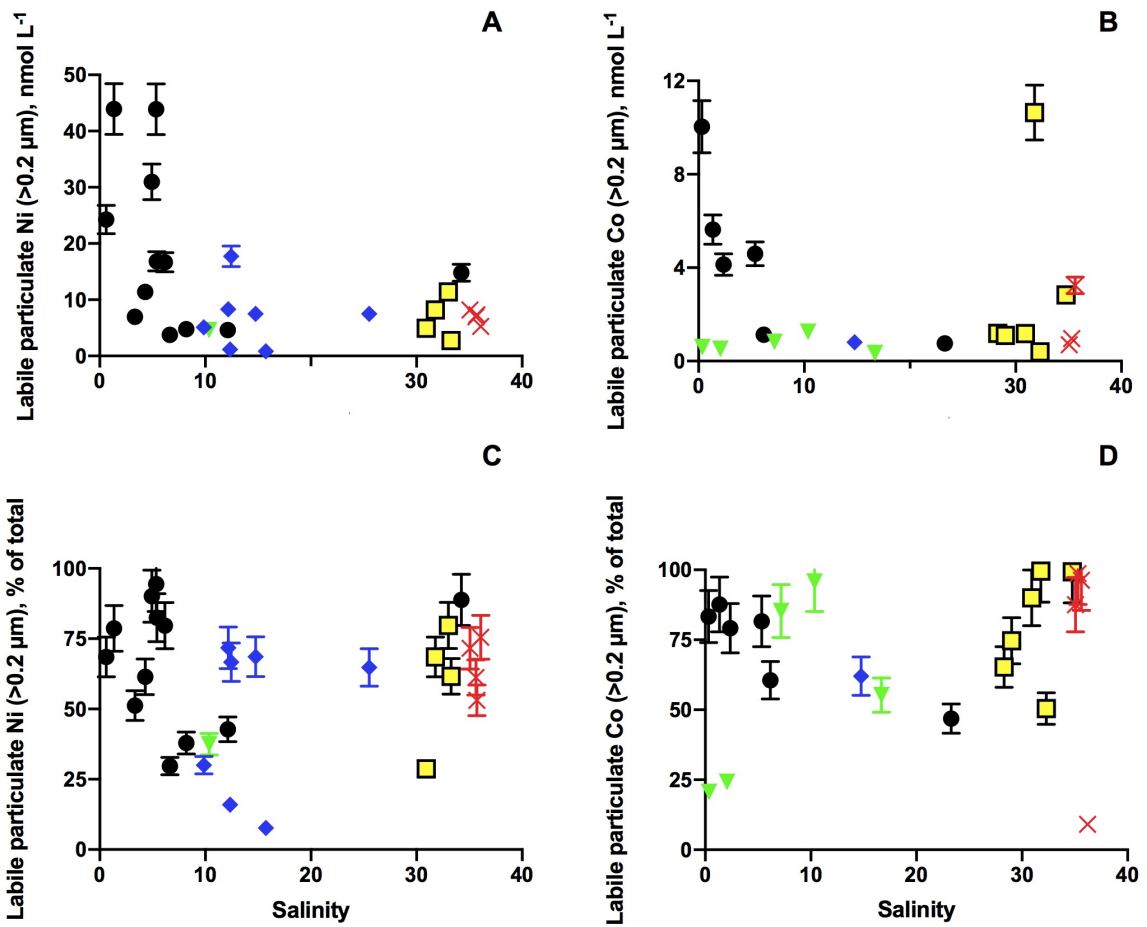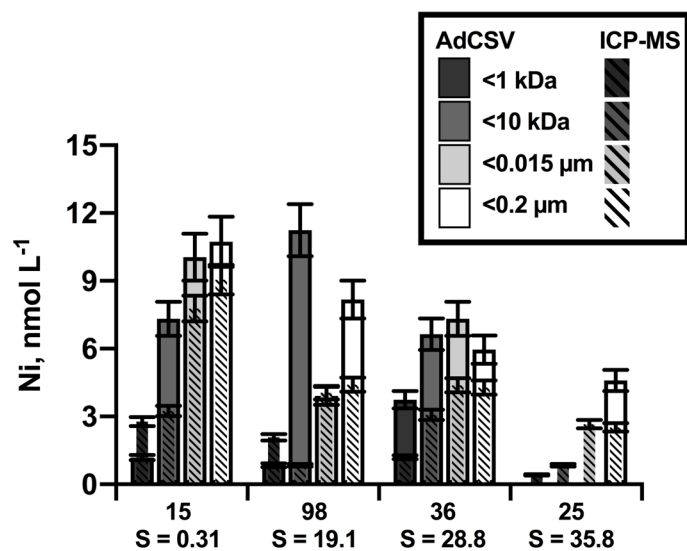
Figure 6: Labile particulate (>0.2 µm) Ni and Co expressed as concentrations **(A-B)** and percent of total **(C-D)** along the mixing zone obtained by AdCSV measurements.
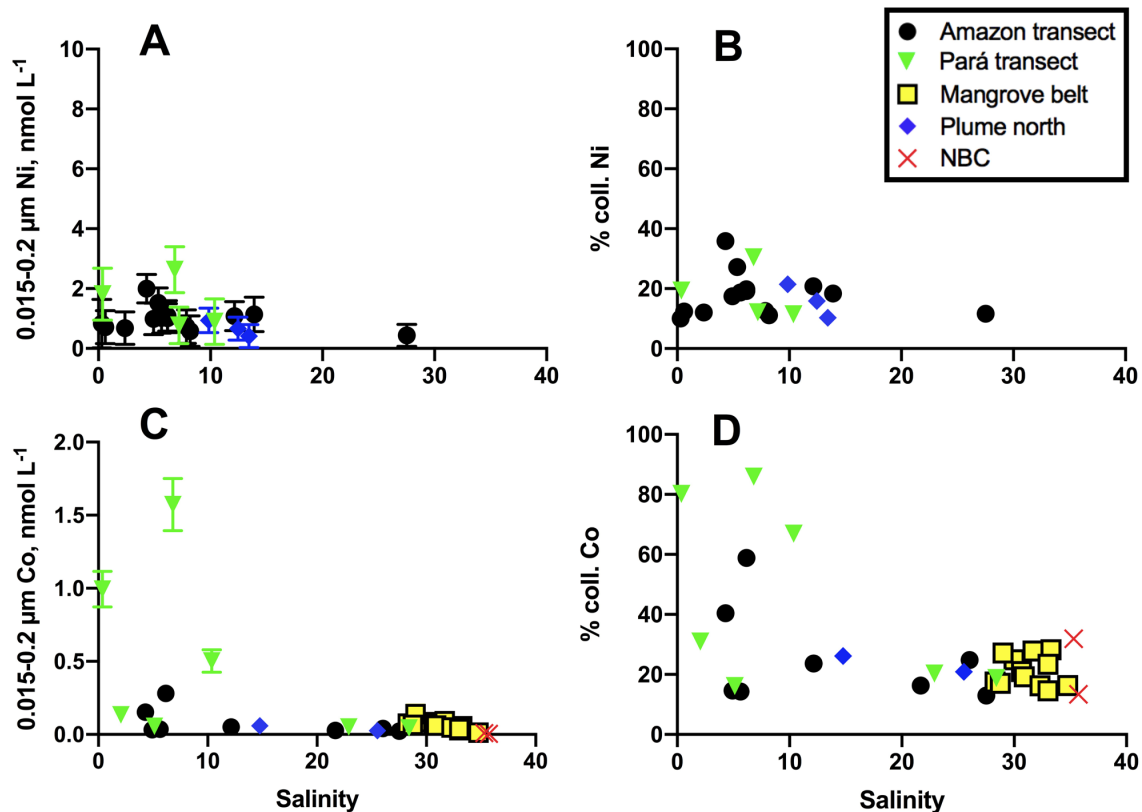
Figure 7: Distribution of large colloidal (0.015-0.2 μm) concentrations (left) and percent of total dissolved (right) for Ni **(A-B)** and Co **(C-D)** obtained by ICP-MS measurements. Colloidal values within error of 0 are not shown.

Figure 8: Comparative distribution of Ni species in four selected samples in the dissolved (<0.2 μm), soluble (<0.015 μm) and ultrafiltered (<1 kDa and <10 kDa) size fractions measured by ICP-MS and AdCSV.

References

Achterberg, E.P., Van den Berg, C.M., 1997. Chemical speciation of chromium and nickel in the western Mediterranean. Deep Sea Res. 44, 693–720. https://doi.org/10.1016/S0967-0645(96)00086-0

Archer, C., Vance, D., Milne, A., Lohan, M.C., 2020. The oceanic biogeochemistry of nickel and its isotopes: New data from the South Atlantic and the Southern Ocean biogeochemical divide. Earth Planet. Sci. Lett. 535, 116–118. https://doi.org/10.1016/j.epsl.2020.116118

Balistrieri, L.S., Murray, J.W., 1986. The surface chemistry of sediments from the Panama Basin: The influence of Mn oxides on metal adsorption. Geochim. Cosmochim. Acta 50, 2235–2243. https://doi.org/10.1016/0016-7037(86)90078-5

Biller, D.V., Bruland, K.W., 2012. Analysis of Mn, Fe, Co, Ni, Cu, Zn, Cd, and Pb in seawater using the Nobias-chelate PA1 resin and magnetic sector inductively coupled plasma mass spectrometry (ICP-MS). Mar. Chem. 130, 12–20. https://doi.org/10.1016/j.marchem.2011.12.001

Boiteau, R.M., Till, C.P., Ruacho, A., Bundy, R.M., Hawco, N.J., McKenna, A.M., Barbeau, K.A., Bruland, K.W., Saito, M.A., Repeta, D.J., 2016. Structural characterization of natural nickel and copper binding ligands along the US GEOTRACES Eastern Pacific Zonal Transect. Frontiers in Marine Sci. 3, 1–16. https://doi.org/10.3389/fmars.2016.00243

Bown, J., Boye, M., Nelson, D. M., 2012. New insights on the role of organic speciation in the biogeochemical cycle of dissolved cobalt in the southeastern Atlantic and the Southern Ocean. Biogeosci., 9, 2719–2736.

Boyd, P. W., M. J. Ellwood, A. Tagliabue, and B. S. Twining, 2017. Biotic and abiotic retention, recycling and remineralization of metals in the ocean. Nat. Geosci. 10, 167–173. https://doi:10.1038/ngeo2876

Boyle E.A., Edmond J.M., and Sholkovitz E.R., 1977. The mechanism of iron removal in estuaries. Geochim. Cosmochim. Acta 41, 1313–1324. https://doi.org/10.1016/0016-7037(77)90075-8

Boyle, E.A., Huested, S.S., Grant, B., 1982. The chemical mass balance of the Amazon Plume - II. Copper, nickel, and cadmium. Deep Sea Res. 29, 1355–1364. https://doi.org/10.1016/0198-0149(82)90013-9

Browning, T.J., Achterberg, E.P., Rapp, I., Engel, A., Bertrand, E.M., Tagliabue, A., Moore, C.M., 2017. Nutrient co-limitation at the boundary of an oceanic gyre. Nature 551, 242–246. https://doi.org/10.1038/nature24063

Bruland, K.W., 1980. Oceanographic distributions of cadmium, zinc, nickel, and copper in the North Pacific. Earth Planet. Sci. Lett. 47, 176–198. https://doi.org/10.1016/0012-821X(80)900

Bundy, R.M., Tagliabue, A., Hawco, N.J., Morton, P.L., Twining, B.S., Hatta, M., Noble, A.E., Cape, M.R., John, S.G., Cullen, J.T. and Saito, M.A., 2020. Elevated sources of cobalt in the Arctic Ocean. Biogeosciences, 17, 4745–4767. https://doi.org/10.5194/bg-17-4745-2020

Byrne, R.H., Kump, L.R., Cantrell, K.J., 1988. The influence of temperature and pH on trace metal speciation in seawater. Marine Chem. 25, 163–181. https://doi.org/10.1016/0304-4203(88)90062-X

Cabanesa, D.J.E., Norman, L., Bowie, A.R., Strmečki, S., Hassler, C.S., 2020. Electrochemical evaluation of iron-binding ligands along the Australian GEOTRACES southwestern

Pacific   section   (GP13).   Marine   Chem.   219,   103736. https://doi.org/10.1016/j.marchem.2019.103736

Carvalho, L.M., Spengler, C., Garmatz, J.C., Nascimento, P.C., Bohrer, D., Delfabro, L., Radis, G., Bolli, A.A., 2008. Voltammetric determination of metals in waters and biological fluids using sample mineralization with ultraviolet radiation. Quím. Nova 31, 1336–1342. https://doi.org/10.1590/S0100-40422008000600012

Cesar, R., Egler, S., Polivanov, H., Castilhos, Z., Rodrigues, A.P., 2011. Mercury, copper and zinc contamination in soils and fluvial sediments from an abandoned gold mining area in southern Minas Gerais State, Brazil. Environ. Earth Sci. 64, 211–222. https://doi.org/10.1007/s12665-010-0840-8

Coleman, J.S., 1966. Chloride complexes of cobalt(II) in anion and cation exchangers. J. Inorg. Nu¢l. Chem. 28, 2371–2378.

Ćosović, B., Degobbis, D., Bilinski, H., Branica, M., 1982. Inorganic cobalt species in seawater. Geochim.   Cosmochim.   Acta   46,   151–158.   https://doi.org/10.1016/0016-7037(82)90242-3

Davidson, E.A., de Araújo, A.C., Artaxo, P., Balch, J.K., Brown, I.F., Bustamante, M.M., Coe, M.T., DeFries, R.S., Keller, M., Longo, M., 2012. The Amazon basin in transition. Nature 481, 321–328. https://doi.org/10.1038/nature10717

DeMaster, D.J., McKee, B.A., Moore, W.S., Nelson, D.M., Showers, W.J., Smith Jr., W.O., 1991. Geochemical processes occurring in the waters at the Amazon river/ocean boundary. Oceanography, April 1991, 15–20. https://doi.org/ 10.5670/oceanog.1991.16

Dittmar, T., Lara, R., 2001. Driving forces behind nutrient and organic matter dynamics in a mangrove tidal creek in North Brazil. Estuar. Coast. Shelf Sci. 52, 249–259. https://doi.org/10.1006/ecss.2000.0743

Dittmar, T., Kattner, G., Lara, R. J., 2001. River or mangrove? Tracing major organic matter sources in tropical Brazilian coastal waters, Marine Chem. 73, 253–271. https://doi.org/10.1016/S0304-4203(00)00110-9

Dittmar, T., Hertkorn, N., Kattner, G., Lara, R.J., 2006. Mangroves, a major source of dissolved organic carbon to the oceans, Global Biogeochem. Cycles 20, GB1012, https://doi.org/10.1029/2005GB002570.

Donat, J.R., Lao, K.A., Bruland, K.W., 1994. Speciation of dissolved copper and nickel in South San Francisco Bay: a multi-method approach. Anal. Chim. Acta 284, 547–571. https://doi.org/10.1016/0003-2670(94)85061-5

Duckworth, O.W., Bargar, J.R., Jarzecki, A.A., Oyerinde, O., Spiro, T.G., Sposito, G., 2009. The exceptionally stable cobalt (III)-desferrioxamine B complex. Marine Chem. 113, 114–122.

Dulaquais, G., Boye, M., Middag, R., Owens, S., Puigcorbe, V., Buesseler, K., Masqué, P., De Baar, H.J., Carton, X., 2014. Contrasting biogeochemical cycles of cobalt in the surface western Atlantic Ocean. Global Biogeochemical Cycles. 28, 1387–1412.

Dupont, C.L., Buck, K.N., Palenik, B., Barbeau, K., 2010. Nickel utilization in phytoplankton assemblages from contrasting oceanic regimes. Deep Sea Res. 57, 553–566.

Dyrssen, D., Krasovec, F., Sillen, L.G., 1959. On the complex formation of nickel with dimethylglyoxime.   Acta   Chem.   Scand.   13,   50–59.   https://doi.org/ 10.3891/acta.chem.scand.07-0663

Ellwood, M.J., van den Berg, C.M., 2001. Determination of organic complexation of cobalt in seawater by cathodic stripping voltammetry. Marine Chem. 75, 33–47. https://doi.org/10.1016/S0304-4203(01)00024-X

Espinoza Villar, J.C., Guyot, J.L., Ronchail, J., Cochonneau, G., Filizola, N., Fraizy, P., Vauchel, P., 2009. Contrasting regional discharge evolutions in the Amazon basin (1974–2004). J. Hydrol. 375, 297–311. https://doi.org/10.1016/j.jhydrol.2009.03.004

Fu, J., Tang, X.-L., Zhang, J., Balzer, W., 2013. Estuarine modification of dissolved and particulate trace metals in major rivers of East-Hainan, China. Contin. Shelf Res. 57, 59–72. https://doi.org/10.1016/j.csr.2012.06.015

Guimberteau, M., Ciais, P., Ducharne, A., Boisier, J.P., Aguiar, A.P.D., Biemans, H., De Deurwaerder, H., Galbraith, D., Kruijt, B., Langerwisch, F., 2017. Impacts of future deforestation and climate change on the hydrology of the Amazon Basin: a multi-model analysis with a new set of land-cover change scenarios. Hydrol. Earth Sys. Sci. 21, 1455–1475. https://doi.org/10.5194/hess-21-1455-2017

Hawco, N.J., Ohnemus, D.C., Resing, J.A., 2016. Twining BS, Saito MA. A dissolved cobalt plume in the oxygen minimum zone of the eastern tropical South Pacific. Biogeosciences. 13, 5697–5717.

Hawco, N.J., Lam, P.J., Lee, J.-M., Ohnemus, D.C., Noble, A.E., Wyatt, N.J., Lohan, M.C., Saito, M.A., 2018. Cobalt scavenging in the mesopelagic ocean and its influence on global mass balance: Synthesizing water column and sedimentary fluxes. Marine Chem. 201, 151–166. https://doi.org/10.1016/j.marchem.2017.09.001

Hollister, A. P., Kerr, M., Malki, K., Muhlbach, E., Robert, M., Tilney, C. L., Breitbart, M., Hubbard, K. A., Buck, K. N., 2020. Regeneration of macronutrients and trace metals during phytoplankton decay: An experimental study. Limnol. Oceanogr. 65, 1936–1960. https://doi.org/10.1002/lno.11429.

Hollister A.P., Whitby, H., Seidel, M., Lodeiro, P., Gledhill, M., Koschinsky, A., 2021. Dissolved concentrations and organic speciation of copper in the Amazon River estuary and mixing plume. Mar. Chem. 243, 104005. https://doi.org/10.1016/j.marchem.2021.104005

Hunter, A.H., 1983. On the estuarine mixing of dissolved substances in relation to colloid stability and surface properties. Geochim. Cosmochim. Acta 47, 467–473. https://doi.org/10.1016/0016-7037(83)90269-7

Koschinsky, A., 2018 – METEOR-Berichte Interactions of trace metals, DOM, and particles in the Amazon estuary and associated plume as key processes for trace metal and DOM fluxes into the Atlantic (Cruise report M147) https://www.tib.eu/en/search/id/awi%3Adoi~10.2312%252Fcr_m147/

Lacerda, L.D., de Souza, M., Ribeiro, M.G., 2004. The effects of land use change on mercury distribution in soils of Alta Floresta, Southern Amazon. Environ. Pollut. 129, 247–255. https://doi.org/10.1016/j.envpol.2003.10.013

Lee, B.G., Fisher, N.S., 1993. Microbially mediated cobalt oxidation in seawater revealed by radiotracer experiments. Limnol. Oceanogr. 38, 1593–1602. https://doi.org/10.4319/lo.1993.38.8.1593

Martell, A.E., Smith, R.M. Critical stability constants. Plenum Press, New York and London, 1989.

Melfi, A.J., Trescases, J.-J., Carvalho, A., de Oliveira, S.M.B., Ribeiro Filho, E., Formoso, M.L.L., 1988. The lateritic ore deposits of Brazil. Sci. Geol. Bull. 41, 5–36.

Middag, R., de Baar, H.J., Bruland, K.W., van Heuven, S.M., 2020. The distribution of nickel in the West-Atlantic Ocean, its relationship with phosphate and a comparison to cadmium and zinc. Frontiers in Marine Sci. 7, 1–17. https://doi.org/10.3389/fmars.2020.00105

Milne, A., Landing, W., Bizimis, M., Morton, P., 2010. Determination of Mn, Fe, Co, Ni, Cu, Zn, Cd and Pb in seawater using high resolution magnetic sector inductively coupled mass spectrometry (HR-ICP-MS). Anal. Chim. Acta 665, 200–207. https://doi.org/10.1016/j.aca.2010.03.027

Morris, D.F.C., Reed, G.L., Short, E.L., Slater, D.N., Waters, D.N., 1965. Nickel(II) chloride complexes in aqueous solution. J. Inorg. Nu¢l. Chem. 27, 377–382.

Mosley, L.M., Liss, P.S., 2020. Particle aggregation, pH changes and metal behaviour during estuarine mixing: review and integration. Marine Freshwater Res. 71, 300–310. https://doi.org/10.1071/MF19195

Motekaitis, R.; Martell, A.E., 1987. Speciation of metals in the oceans. I. Inorganic complexes in seawater, and influence of added chelating agents Marine Chem. 21, 101–116. https://doi.org/10.1016/0304-4203(87)90032-6

Muratt, D.T., Carvalho, L.M., Viana, C., Nascimento, P.C., Reis, G., Dal Molin, T.R., Grassmann, C., Smidt, G., Koschinsky, A., 2015. Sequential determination of 13 elements in complex matrices by stripping voltammetry with mixed complexing electrolytes. Electroanal. 27, 1625–1635. https://doi.org/10.1002/elan.201500089

Nimmo, M., van den Berg, C.M.G., Brown, J., 1989. The chemical speciation of dissolved nickel, copper, vanadium and iron in Liverpool Bay, Irish Sea. Est. Coast. Shelf Sci. 29, 57–74. https://doi.org/10.1016/0272-7714(89)90073-5

Noble, A.E., Ohnemus, D.C., Hawco, N.J., Lam, P.J., Saito, M.A., 2017. Coastal sources, sinks and strong organic complexation of dissolved cobalt within the US North Atlantic GEOTRACES transect GA03. Biogeosciences. 14, 2715–2739. https://doi.org/10.5194/bg-14-2715-2017

Oldham, V.E., Miller, M.T., Jensen, L.T., Luther III, G.W., 2017. Revisiting Mn and Fe removal in humic rich estuaries. Geochim. Cosmochim. Acta 209, 267–283. https://doi.org/10.1016/j.gca.2017.04.001

Oliveira, S.M.B., Trescases, J.-J., Melfi, A.J., 1992. Lateritic nickel deposits of Brazil. Mineral. Deposita 27, 137–146. https://doi.org/10.1007/BF00197099

Pöhle, S., Schmidt, K., Koschinsky, A., 2015. Determination of Ti, Zr, Nb, V, W and Mo in seawater by a new online-preconcentration method and subsequent ICP-MS analysis, Deep Sea Res. I 98, 83–93. https://doi.org/10.1016/j.dsr.2014.11.014

Price, N. M., Morel, F. M. M., 1991. Colimitation of phytoplankton growth by nickel and nitrogen. Limnol. Oceanogr. 36, 1071–1076. https://doi.org/10.4319/lo.1991.36.6.1071

Rapp, I., Schlosser, C., Rusiecka, D., Gledhill, M., Achterberg, E.P., 2017. Automated preconcentration of Fe, Zn, Cu, Ni, Cd, Pb, Co, and Mn in seawater with analysis using high-resolution sector field inductively-coupled plasma mass spectrometry. Anal. Chim. Acta. 976, 1–13. https://doi.org/10.1016/j.aca.2017.05.008

Revels, B. N., Rickli, J., Moura, C. A. V., Vance, D., 2021. Nickel and its isotopes in the Amazon Basin: the impact of the weathering regime and delivery to the oceans. Geochim. Cosmochim. Acta, 293, 344–364. https://doi.org/10.1016/j.gca.2020.11.005

Sadat-Noori, M., and Glamore, W., 2019. Porewater exchange drives trace metal, dissolved organic carbon and total dissolved nitrogen export from a temperate mangrove wetland. J. Environ. Management, 248, 109264. https://doi.org/10.1016/j.jenvman.2019.109264

Saito, M.A., Moffett, J.W., 2001. Complexation of cobalt by natural organic ligands in the Sargasso Sea as determined by a new high-sensitivity electrochemical cobalt speciation method suitable for open ocean work. Marine Chem. 75, 49–68. https://doi.org/10.1016/S0304-4203(01)00025-1

Saito, M.A., Moffett, J.W., Chisholm, S.W., Waterbury, J.B., 2002. Cobalt limitation and uptake in *Prochlorococcus.* Limnol. Oceanogr. 47, 1629–1636. https://doi.org/10.4319/lo.2002.47.6.1629

Saito, M.A., Goepfert, T.J., 2008. Zinc-cobalt colimitation of *Phaeocystis antarctica.* Limnol. Oceanogr. 53, 266–275. https://doi.org/10.4319/lo.2008.53.1.0266.

Sander, S., Koschinsky, A., 2000. Onboard-ship redox speciation of chromium in diffuse hydrothermal fluids from the North Fiji Basin. Marine Chem. 71, 83–102. https://doi.org/ 10.1016/S0304-4203(00)00042-6

Sarbolouki, M.N., 1982. A general diagram for estimating pore size of ultra ltration and reverse osmosis membranes. Sep. Sci. Technol. 17, 381–386. https://doi.org/ 10.1080/01496398208068547.

Sclater, F., Boyle, E., Edmond, J., 1976. On the marine geochemistry of nickel. Earth Planet. Sci. Lett. 31, 119–128. https://doi.org/10.1016/0012-821X(76)90103-5

Seyler, P.T., Boaventura, G.R., 2003. Distribution and partition of trace metals in the Amazon basin. Hydrol. Proc. 17, 1345–1361. https://doi.org/10.1002/hyp.1288

Sholkovitz, E.R., 1978. The flocculation of dissolved Fe, Mn, Al, Cu, Ni, Co and Cd during estuarine mixing. Earth Planet. Sci. Lett. 41, 77–86. https://doi.org/10.1016/0012-821X(78)90043-2

Sholkovitz, E.R., Price, N.B., 1980. The major-element chemistry of suspended matter in the Amazon estuary. Geochim. Cosmochim. Acta 44, 163–171. https://doi.org/ 10.1016/0016-7037(80)90128-3

Sholkovitz, E.R., 1993. The geochemistry of rare earth elements in the Amazon River estuary. Geochim. Cosmochim. Acta 57, 2181–2190. https://doi.org/10.1016/0016-7037(93)90559-F

Smoak, J.M., Krest, J.M., Swarzenski, P.W., 2006. Geochemistry of the Amazon Estuary. In: Handbook of Environmental Chemistry Vol. 5, Part H, pp. 71–90, Springer-Verlag, Berlin, Heidelberg. https://doi.org/10.1007/6985029.

Sohrin, Y., Urushihara, S., Nakatsuka, S., Kono, T., Higo, E., Minami, T., Norisuye, K., Umetani, S., 2008. Multielemental determination of GEOTRACES key trace metals in seawater by ICPMS after preconcentration using an ethylenediaminetriacetic acid chelating resin. Anal. Chem. 80, 6267–6273. https://doi.org/10.1021/ac800500f

Stolpe, B., Hassellöv, M., 2007. Changes in size distribution of freshwater nanoscale colloidal matter and associated elements on mixing with seawater. Geochim. Cosmochim. Acta 71, 3292–3301. https://doi.org/10.1016/j.gca.2007.04.025

Suhrhoff, T.J., Rickli, J., Crocket, K., Bura-Nakic, E., Vance, D., 2019. Behavior of beryllium in the weathering environment and its delivery to the ocean. Geochim. Cosmochim. Acta 265, 48–68. https://doi.org/10.1016/j.gca.2019.08.017

Sunda, W.G.; Huntsman, S.A., 1987. Microbial oxidation of manganese in a North Carolina estuary. Limnol. Oceanogr. 32, 552–564. https://doi.org/10.4319/lo.1987.32.3.0552

Swarzensky, P.W., Booth, J.G., 1995. Uranium geochemistry on the Amazon shelf: chemical phase partitioning and cycling across a salinity gradient. Geochim. Cosmochim. Acta, 59, 7–18. https://doi.org/10.1016/0016-7037(94)00371-R

Tani, Y., Ohashi, M., Miyata, N., Seyama, H., Iwahori, K., Soma, M., 2004. Sorption of Co (II), Ni (II), and Zn (II) on biogenic manganese oxides produced by a Mn-oxidizing fungus, strain KR21-2. J. Environ. Sci. Health A 39, 2641–2660. https://doi.org/10.1081/ESE-200027021

Tebo, B.M., Nealson, K.H., Emerson, S., Jacobs, L., 1984. Microbial mediation of Mn (II) and Co (II) precipitation at the O2/H2S interfaces in two anoxic fjords. Limnol. Oceanogr. 29, 1247–1258. https://doi.org/10.4319/lo.1984.29.6.1247

Thanh-Nhoab, N.; Strady, E.; Nhu-Trang, T-T.; David, F.; Marchand, C., 2018. Trace metals partitioning between particulate and dissolved phases along a tropical mangrove estuary (Can Gio, Vietnam). Chemosphere 196, 311–322. https://doi.org/10.1016/j.chemosphere.2017.12.189

Tremblay, L.B., Dittmar, T., Marshall, A.G., Cooper, W.J., Cooper, W.T., 2007. Molecular characterization of dissolved organic matter in a North Brazilian mangrove porewater and mangrove-fringed estuaries by ultrahigh resolution Fourier Transform-Ion Cyclotron Resonance mass spectrometry and excitation/emission spectroscopy. Marine Chem. 105, 15–29. https://doi.org/10.1016/j.marchem.2006.12.015

Van den Berg, C.M. ., Nimmo, M., 1987. Determination of interactions of nickel with dissolved organic material in seawater using cathodic stripping voltammetry. Sci. Tot. Environ. 60, 185–195. https://doi.org/10.1016/0048-9697(87)90415-3

Yamasoe, M.A., Artaxo, P., Miguel, A.H., Allen, A.G., 2000. Chemical composition of aerosol particles from direct emissions of vegetation fires in the Amazon Basin: water-soluble species and trace elements. Atmospher. Environ. 34, 1641–1653. https://doi.org/10.1016/S1352-2310(99)00329-5

Xue, H.B., Jansen, F., Prasch, A., Sigg, L., 2001. Nickel speciation and complexation kinetics in freshwater by ligand exchange and DPCSV. Environ. Sci. Technol., 35, 539–546. https://doi.org/10.1021/es0014638

Zhang, Z., Cao, Z., Grasse, P., Dai, M., Gao, L., Kuhnert, H., Gledhill, M., Chiessi, C.M., Doering, K., Frank, M., 2020. Dissolved silicon isotope dynamics in large river estuaries. Geochim. Cosmochim. Acta 273, 367–382. https://doi.org/10.1016/j.gca.2020.01.028